4478 *Inorg. Chem.* **2010**, *49*, 4478–4485
DOI: 10.1021/ic100042z

Inorganic Chemistry
Article

Dense Yttria Phase Eclipsing the A-Type Sesquioxide Structure: High-Pressure Experiments and ab initio Calculations

Hitoshi Yusa,*,† Taku Tsuchiya,‡ Nagayoshi Sata,§ and Yasuo Ohishi¶

†*National Institute for Materials Science* (*NIMS*), *1-1 Namiki, Tsukuba 305-0044, Japan,* ‡*Geodynamics Research Center* (*GRC*), *Ehime University, 2-5 Bunkyo-cho, Matsuyama 790-8577, Japan,* §*Institute for Frontier Research on Earth Evolution* (*IFREE*), *Japan Agency for Marine-Earth Science and Technology*(*JAMSTEC*), *2-15 Natsushima-cho, Yokosuka 237-0061, Japan, and* ¶*Japan Synchrotron Radiation Research Institute* (*JASRI*), *1-1-1 Kouto, Sayo-cho 679-5198, Japan*

Received January 8, 2010

In situ X-ray diffraction experiments and ab initio calculations elucidated the high-pressure phase transition properties of yttrium sesquioxides. The C-, B-, and A-type sesquioxides structure sequence observed in the room-temperature compression does not coincide with the high-pressure phase sequence of yttrium sesquioxides at high temperature. A reconstructive-type transformation taking place at high temperature yields the Gd_2S_3 structure around 8 GPa with a drastic change in cation-oxygen coordinations. Ab initio structural optimization suggests that a displacive-type transformation from B- to A-type sesquioxides structure metastably occurs under pressure at room temperature. The calculated density of states indicates that the transition to the Gd_2S_3 structure causes a significant decrease in the band gap. The Gd_2S_3 phase was also found to be partially recovered at ambient pressure. We briefly discuss the quenchability of the Gd_2S_3 structure in sesquioxides on the basis of the enthalpy differences between the ambient phase and the recovered products.

Introduction

Yttria (Y_2O_3) is widely used in heat-resistant ceramics and as a key component of functional materials such as yttria stabilized zirconia for solid-oxide fuel cells.[1] Yttria has a similar ionic radius (Y^{3+} = 0.90 Å) to that of lanthanides (Ln^{3+} = 0.86−1.03 Å),[2] so that lanthanide ions can be incorporated into it to make optical ceramics such as Eu^{3+}:Y_2O_3 red-emitting phosphor[3,4] and Nd^{3+}:Y_2O_3[5] and Yb^{3+}:Y_2O_3[6] lasers. Indeed, under ambient conditions, yttria crystallizes into a bixbyite structure (C-type rare earth sesquioxide structure, denoted as C-RES hereafter) like those of lanthanide sesquioxides (Ln_2O_3). The high-pressure phase was confirmed to be B-RES in samples recovered from static high-pressure experiments at 2.5 GPa and 1273 K[7,8] and shock compression experiments conducted above 12 GPa and below 673 K.[9] However, even the latter experiments did not detect the A-RES phase, which is expected to be a part of the phase transformation sequence of lanthanide sesquioxides. In situ observations using X-ray diffraction[10] and Raman scattering experiments[11] conducted at room temperature reported a phase transformations to the missing A-RES phase, although there have been some disagreements among researchers on the transformation process. High-pressure Raman spectra[11] indicated stepwise transitions from C- to B-RES at 12 GPa and from B- to A-RES at 19 GPa with increasing pressure. In contrast, the high-pressure X-ray study of Y_2O_3 by Wang et al.[10] concluded that C-RES directly transforms into A-RES at 12.1 GPa without going through the B-RES, whereas the transformation sequence of C, B, to A was only observed in Eu^{3+}:Y_2O_3. It was, in addition, reported that a high-temperature phase (CaF_2 type) in Y_2O_3 formed at 2493 K, which is just below the melting point, under ambient pressure.[12,13] To the best of our knowledge, however, there are no in situ high-pressure

*E-mail: yusa.hitoshi@nims.go.jp.

(1) Yamamoto, O. *Electrochim. Acta* **2000**, *45*, 2423.
(2) Shannon, R. D. *Acta Crystallogr. A* **1976**, *32*, 751; We quoted the trivalent cationic radii with six coordination number from this article.
(3) Wickersheim, K. A.; Lefever, R. A. *J. Electrochem. Soc*. **1964**, *111*, 47.
(4) Jones, S. L.; Kumar, D.; Singh, R. K.; Holloway, P. H. *Appl. Phys. Lett*. **1997**, *71*, 404.
(5) Lu, J.; Lu, J.; Murai, T.; Takaichi, K.; Uematsu, T.; Ueda, K.; Yagi, H.; Yanagitani, T.; Kaminskii, A. A. *Jpn. J. Appl. Phys*. **2001**, *40*, L1277.
(6) Lu, J.; Takaichi, K.; Uematsu, T.; Shirakawa, A.; Musha, M.; Ueda, K.; Yagi, H.; Yanagitani, T.; Kaminskii, A. A. *Jpn. J. Appl. Phys*. **2002**, *41*, L1373.
(7) Hoekstra, H. R.; Gingerich, K. A. *Science* **1964**, *146*, 1163.
(8) Hoekstra, H. R. *Inorg. Chem*. **1966**, *5*, 754.
(9) Atou, T.; Kusaba, K.; Fukuoka, K.; Kikuchi, M.; Syono, Y. *J. Solid State Chem*. **1990**, *89*, 378.
(10) Wang, L.; Pan, Y.; Ding, Y.; Yang, W.; Mao, W. L.; Sinogeikin, S. V.; Meng, Y.; Shen, G.; Mao, H. K. *Appl. Phys. Lett*. **2009**, *94*, 061921.
(11) Husson, E.; Proust, C.; Gillet, P.; Itie, J. P. *Mater. Res. Bull*. **1999**, *34*, 2085.
(12) Katagiri, S.; Ishizawa, N.; Marumo, F. *Powder Diffraction* **1993**, *8*, 60.
(13) Swamy, V.; Dubrovinskaya, N. A.; Dubrovinsky, L. S. *J. Mater. Res*. **1999**, *14*, 456.

 Published on Web 04/16/2010

experiments showing temperature effects on phase transformations in Y_2O_3.

A recent topic in high-pressure crystallography of III sesquioxides regards their dense structures.[14−16] Umemoto and Wentzcovitch[14] theoretically predicted the U_2S_3 structure would form in Al_2O_3 at 370 GPa as a post-$CaIrO_3$ phase. In contrast, we experimentally discovered the Gd_2S_3 structure in In_2O_3 at 40 GPa after heating at 1500−2000 K and confirmed the stabilization of this phase as a post-Rh_2O_3 (II) structure by ab initio calculations.[15] The U_2S_3 and Gd_2S_3 structures both possess seven and eight oxygen coordinations, which are higher than those in the corundum, $CaIrO_3$, and Rh_2O_3(II) structures. Very recently, a Gd_2S_3 structure also found in Sc_2O_3, belonging to a group of IIIA sesquioxides, in the high-pressure phase evolution from B-RES.[16] Although we could not experimentally confirm the presence of A-RES in Sc_2O_3, the density increase from B-RES to the Gd_2S_3 phase could exceed the estimated density change from B- to A-RES. In this study, we search for a phase denser than A-RES in Y_2O_3 to elucidate its high-pressure phase relationship by using in situ X-ray diffraction methods under high $P-T$ conditions and also density functional ab initio calculations.

Experimental Section

Powdered Y_2O_3 sample (99.999% pure: Aldrich P/N 204927) mixed with a small amount of gold powder (less than 0.1 wt %) was prepared for high pressure experiments after drying at 873 K for 3 h. A symmetric diamond anvil cell (DAC) was used to apply the pressure to the samples. The samples were loaded into 100−150 μm-diameter holes in 50−70 μm-thick rhenium gaskets with a hydrostatic pressure medium (methanol:ethanol:water = 16:3:1) for the room-temperature compression and without a pressure medium for the laser heating experiments. The in situ high-pressure X-ray diffraction experiments at room temperature and at high temperature were conducted at BL04B2 and BL10XU at SPring8 (JASRI), respectively. Monochromatic synchrotron X-rays tuned to 30 or 38 keV were focused on the sample in the DAC to a spot ~50 μm in diameter. Diffracted X-rays were detected by using imaging plates (IP) and a charge-coupled device (CCD). The Debye rings recorded on the detectors were converted to intensity vs 2θ data by using the FIT2D program.[17] The Nd:YLF laser heating experiments used a beam focused on a spot that was 20 μm in diameter on the sample in the DAC. The temperature was monitored by measuring the gray body radiation emitted from the sample. The maximum temperature was approximately 2000 K. The X-ray data was mainly collected at room temperature after laser heating. We did not detect any phase stabilizing only at high temperature under pressure. Pressure was determined from the lattice parameters of gold.[18]

Ab initio static lattice energy computations were performed within the framework of density functional theory (DFT)[19] with the local density approximation (LDA)[20,21] and the generalized gradient approximation (GGA)[22] implemented in the pwscf code.[23] Ultrasoft pseudopotentials for yttrium and oxygen were nonempirically generated using the methods of Vanderbilt.[24] A plane wave basis set with a cutoff of 50 Ry was chosen to compute the electronic structures of Y_2O_3 polymorphs. The irreducible parts of the Brillouin zone were sampled on 2 × 2 × 2 (2 points), 2 × 4 × 2 (4 points), 4 × 4 × 2 (5 points), 4 × 4 × 4 (10 points), 4 × 4 × 2 (8 points), 4 × 4 × 2 (6 points), 4 × 4 × 2 (4 points), and 2 × 4 × 2 (2 points) Monkhorst-Pack meshes[25] for C-RES, B-RES, A-RES, corundum, Rh_2O_3(II), $CaIrO_3$, Gd_2S_3, and U_2S_3 structures, respectively. All structural degrees of freedom were optimized using constant-pressure damped variable cell-shape molecular dynamics until residual forces became less than 1.0×10^{-5} Ry/au. The effects of using a larger cutoff and a greater number of k points on the calculated properties were found to be insignificant.

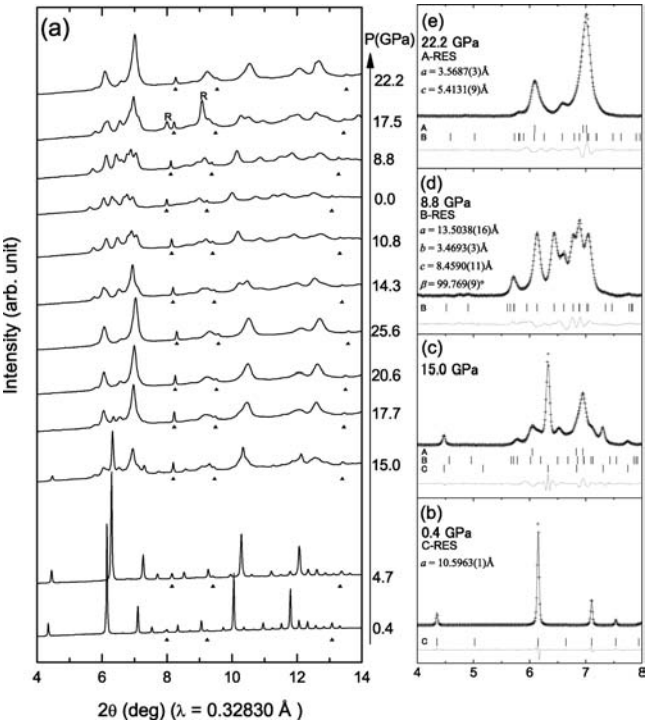

Figure 1. (a) X-ray diffraction profiles from Y_2O_3 samples under room-temperature compression using quasi-hydrostatic pressure medium. Triangles indicate the positions of diffractions from gold powder. *R* indicates the peaks from rhenium gasket. (b−e) Enlargements of the low angle parts in the several diffraction profiles of a and their profile-fitted pattern with LeBail method (GSAS).[26] The difference (dotted line) between the observed (crosses) and fitted patterns (thin line) is shown in the same scale. Tick marks represent the calculated positions of the diffraction peaks of the A-, B-, and C-RES phases as indicated in the figures.

Results and Discussion

Experimental Results. We first reexamined the phase transformation sequence reported in the room temperature compression experiments. The starting C-RES phase was found to turn into a three phase mixture at 15.0 GPa (Figure 1c). Although the structural change from C-RES

(14) Umemoto, K.; Wentzcovitch, R. M. *Proc. Natl. Acad. Sci. U.S.A.* **2008**, *105*, 6526.
(15) Yusa, H.; Tsuchiya, T.; Tsuchiya, J.; Sata, N.; Ohishi, Y. *Phys. Rev. B* **2008**, *78*, 092107.
(16) Yusa, H.; Tsushiya, T.; Sata, N.; Ohishi, Y. *Inorg. Chem.* **2009**, *48*, 7537.
(17) Hammersley, A. P. *FIT2D: An Introduction and overview*. European Synchrotron Radiation Facility Internal Report ESRF97HA02T, **1997**.
(18) Andeson, O. L.; Isaak, D. G.; Yamamoto, S. *J. Appl. Phys.* **1989**, *65*, 1534.
(19) Hohenberg, P.; Kohn, W. *Phys. Rev.* **1964**, *136*, B864.
(20) Ceperley, D. M.; Alder, B. J. *Phys. Rev. Lett.* **1980**, *45*, 566.
(21) Perdew, J. P.; Zunger, A. *Phys. Rev B* **1981**, *23*, 5048.
(22) Perdew, J. P.; Burke, K.; Ernzerhof, M. *Phys. Rev. Lett.* **1996**, *77*, 3865.
(23) http://www.pwscf.org.
(24) Vanderbilt, D. *Phys. Rev. B* **1990**, *41*, 7892.
(25) Monkhorst, H. J.; Pack, J. D. *Phys. Rev. B* **1976**, *13*, 5188.

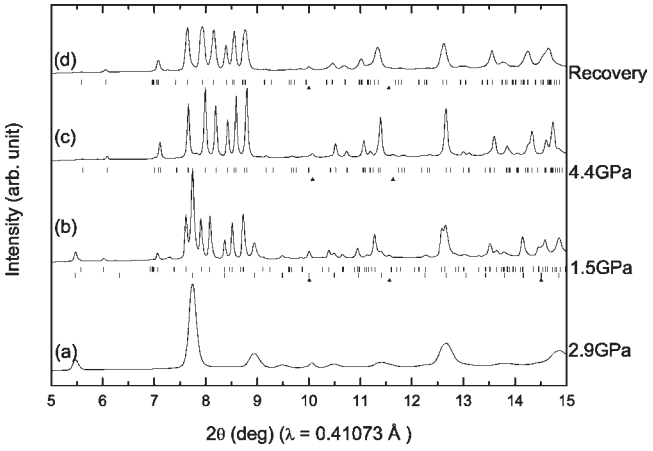

Figure 2. X-ray diffraction profiles from Y_2O_3 samples: (a) after compression to 2.9 GPa, (b) at 1.5 GPa after heating at 1300 ± 150 K, (c) at 4.4 GPa after further heating at 1500 ± 500 K, and (d) after recovery at ambient pressure. Tick marks represent the calculated positions of the diffraction peaks of the C-RES (bottom) and B-RES (top) phases. Triangles indicate the positions of diffractions from gold powder.

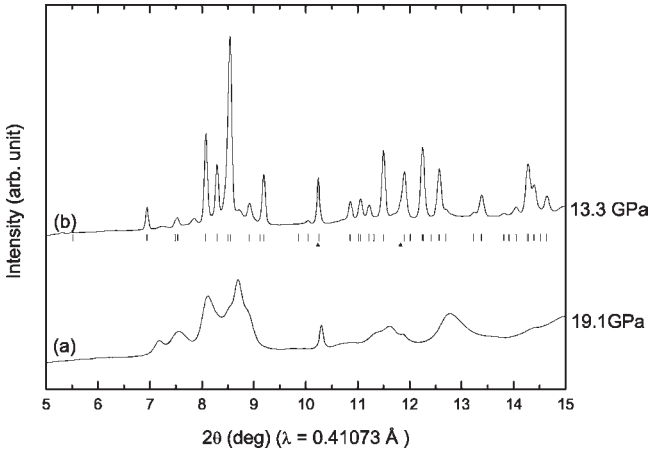

Figure 3. X-ray diffraction profiles from Y_2O_3 samples: (a) after compression to 19.1 GPa and (b) at 13.3 GPa after heating at 1400 ± 200 K. Tick marks represent the calculated positions of the diffraction peaks of the Gd_2S_3 phases. Triangles indicate the positions of diffractions from gold powder.

to A-RES was successfully observed, contrary to the previous X-ray diffraction experiments,[10] the B-RES phase was found to obviously coexist throughout the transition process from the C- to the A-RES phase. After further compression to 25.6 GPa, the sample almost converted to the A-RES phase. Upon decompression, the B-RES phase reappeared at 14.3 GPa and remained as a recovery product at ambient pressure (Figure 1d). Subsequent recompression experiments on this recovered B-RES phase reproduced the A-RES phase above 17.5 GPa (Figure 1e). Considering the multiple phases that metastably appeared in such a wide pressure range, these transitions at room temperature are thought to be kinetically sluggish. In order to investigate the phase changes under equilibrium condition, we next conducted laser annealing experiments under pressure.

In contrast to the sluggish transition under room-temperature compression, the laser heating at 1300 ± 150 K initiates the C- to B-RES transition at 2.9 GPa (Figure 2). After heating, the pressure slightly dropped to 1.5 GPa because of a density increase during the transition. Successive heating at this pressure did not promote the transition any further; therefore, the C- to B-RES transition pressure is estimated to be 1.5 to 2.9 GPa. After a further compression to 5 GPa with heating at 1500 ± 500 K, the remaining C-RES was completely converted into B-RES.

The second heating experiment was started at 19.1 GPa. Without a pressure medium, the X-ray diffraction peaks markedly broadened during a room-temperature compression due to substantial deviatoric stress (Figure 3a). Sharp peaks however appeared in the diffraction profile after laser heating at 1400 ± 200 K (Figure 3b). Though the pressure dropped to 13.3 GPa, we observed a new diffraction pattern, which did not correspond to the B-RES phase. The annealed sample was partially transparent to transmitted light. To identify the new phase and to determine the transition pressure more precisely, two

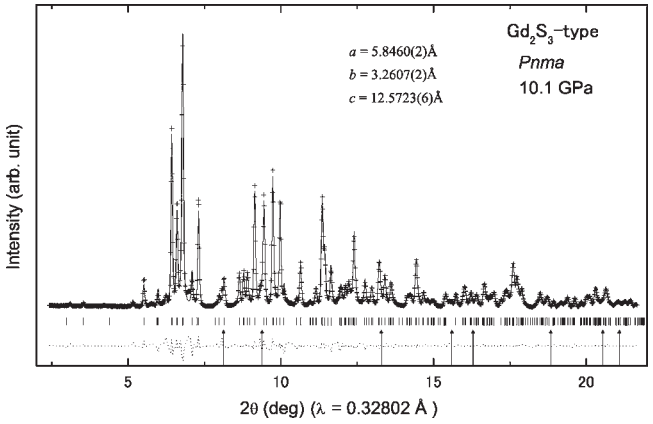

Figure 4. X-ray diffraction profile obtained with the LeBail method (GSAS)[26] for a Gd_2S_3 structure in Y_2O_3 at 10.1 GPa. The difference (dotted line) between the observed (crosses) and fitted patterns (thin line) is shown in the same scale. Tick marks represent the calculated positions of the diffraction peaks of the Gd_2S_3 structure. Arrows indicate the positions of diffractions from gold powder. R_{wp} = 2.6%.

additional laser heating experiments at 2000 ± 500 K were conducted. Then, we performed profile fitting analyses,[26] which obviously show that the pattern obtained at 10.1 GPa can be perfectly assigned by a single phase with the Gd_2S_3 unit cell (Z = 4) and space group (*Pnma*) (Figure 4), whereas the laser-heated sample at about 2000 K and 8.1 GPa was assigned by B-RES. According to these results, we experimentally determined the transition pressure from B-RES to Gd_2S_3 at high temperature to be between 8 and 10 GPa. Laser heating experiments conducted above 30 GPa also yielded a Gd_2S_3 phase stabilizing after a pressure drop to 22.9 GPa (Figure 5b), in contrast to the room-temperature compression which crystallized the A-RES even at 25.6 GPa. In order to confirm the stability of the Gd_2S_3 phase at ambient pressure, we collected an X-ray pattern of the sample after the pressure was fully released. Surprisingly, some diffraction peaks from the Gd_2S_3 phase could still be identified (Figure 5c). Then, we recompressed and heated the same sample to demonstrate a reverse transition from the Gd_2S_3

(26) Larson, A. C.; Von Dreele, R. B. *General Structure Analysis System (GSAS)*. Los Alamos National Laboratory Report LAUR, **2004**; pp 86−748.

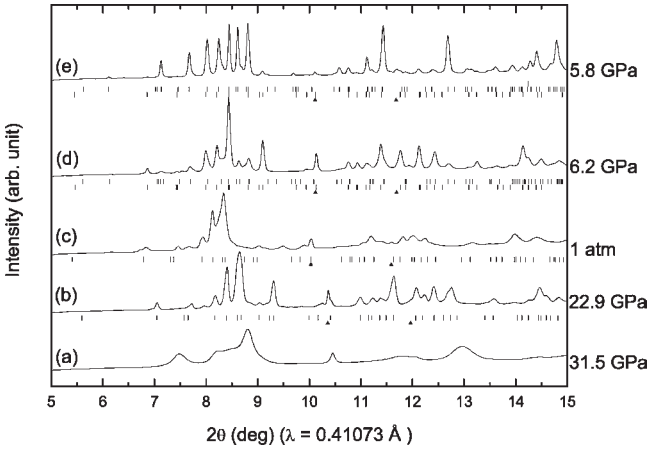

Figure 5. X-ray diffraction profiles from Y_2O_3 samples: (a) after compression to 31.5 GPa, (b) at 22.9 GPa after heating at 1750 ± 200 K, (c) after decompression to ambient pressure, (d) recompressed and heated at 1500 ± 200 K, and (e) reheated at 1600 ± 250 K. Tick marks represent the calculated positions of the diffraction peaks of the Gd_2S_3 (bottom) and B-RES (top) phases. Triangles indicate the positions of diffractions from gold powder.

to the B-RES phase. A small amount of B-RES started to appear in the diffraction pattern at 6.2 GPa after heating at 10.6 GPa. Subsequently, most of the sample converted into the B-RES phase at 5.8 GPa after reheating. On the basis of these reverse transition experiments, we can conclude that the Gd_2S_3 phase stabilizes as the post B-RES phase in the high-temperature conditions.

Computational Results. Static enthalpy differences of B-RES, A-RES, corundum, Rh_2O_3 (II), $CaIrO_3$, Gd_2S_3, and U_2S_3 structures relative to C-RES were calculated up to 60 GPa within DFT combining LDA and GGA (Figure 6). In both calculations, the first phase crossing over the C-RES's enthalpy is B-RES with transition pressures at 2 GPa (LDA) and 7 GPa (GGA). Interestingly, both B-RES's and A-RES's enthalpy lines are found to converge above these transition pressures. We found this behavior can be attributed to the structural similarity between B- and A-RES, which will be described later in detail. In the LDA calculations, the B-RES's enthalpy line approaches A-RES's line at 8 GPa and then the Gd_2S_3's line intersects the A-RES's line near 9 GPa (Figure 6a). In the case of GGA, the B- and A-RES's lines completely converge and the B-RES phase directly transforms to the Gd_2S_3 phase (Figure 6b). Irrespective of the small difference, LDA and GGA both predict the same phase of Gd_2S_3 rather than U_2S_3, whose enthalpy line runs nearly parallel to the Gd_2S_3's line, suggesting no crossing at higher pressures. Enthalpy lines of the corundum, Rh_2O_3(II), and $CaIrO_3$ phases are far higher than those of the B and A-RES phases.

We analyzed the orbital-projected density of states (PDoS) of the A-RES and Gd_2S_3 phases (Figure 7) at 30 GPa in order to understand their bonding properties including energy gaps. In both cases, the upper valence band exhibits similar widths from −5 to 0 eV, which are mainly composed of the O 2p states with a small hybridization of Y 4d states. On the other hand, the position of the conduction band bottom which consists mainly of the Y 4d states is pulled down to 2.6 eV in the Gd_2S_3 phase (Figure 7a), compared to 4.4 eV in the A-RES phase

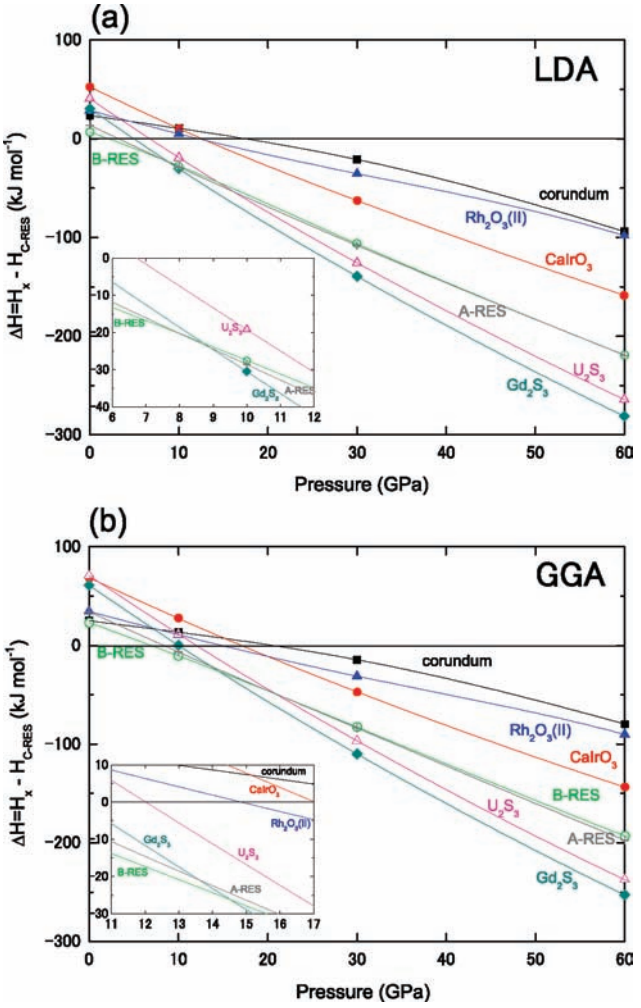

Figure 6. Enthalpy differences relative to C-RES for B-RES (open circles), A-RES (crosses), Gd_2S_3 (diamonds), U_2S_3 (open triangles), $CaIrO_3$ (solid circles), Rh_2O_3(II) (solid triangles), and corundum (squares) in Y_2O_3 by (a) DFT-LDA and (b) DFT-GGA computations under the static condition. The low-pressure parts are enlarged in the insets.

(Figure 7b). A previous theoretical study[27] gave a comparable band gap of 4.54 eV for the C-RES phase; therefore, among Y_2O_3 polymorphs, only the Gd_2S_3 phase exhibits a significantly small band gap. This is primarily due to the high cation−oxygen coordinations in Gd_2S_3. Similarly, a recent DFT study on the Sc_2O_3 polymorphs reported comparable band gaps of 3.885, 3.729, and 3.715 eV for the C-, B-, and A-RES phases, respectively.[28] As being analogous to Y_2O_3, a small band gap would be expected to the Gd_2S_3 phase of Sc_2O_3.

Transition Properties of B- to A-RES and Gd_2S_3 Phases. The calculated phase sequence and the transition pressures are basically in good harmony with the results of the laser heating experiments. Although the experimental transition pressures often locate between the LDA (lower) and GGA (higher) transition pressures in many cases,[15,16] those seem closer to the LDA values in the present case. On the other hand, some disagreements are clearly seen with the results of the room temperature compression experiments. We experimentally observed

(27) Xu, Y. N.; Gu, Z. q.; Ching, W. Y. *Phys. Rev. B* **1997**, *56*, 14993.
(28) Liu, D.; Lei, W.; Li, Y.; Ma, Y.; Hao, J.; Chen, X.; Jin, Y.; Liu, D.; Yu, S.; Cui, Q.; Zou, G. *Inorg. Chem.* **2009**, *48*, 8251.

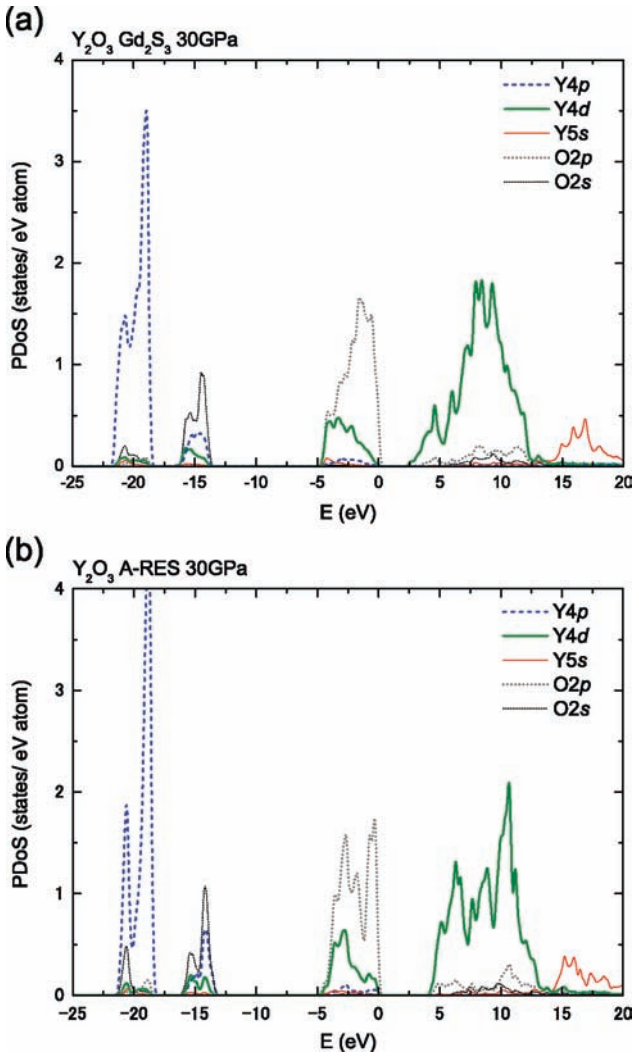

Figure 7. Projected density of states (PDoS) of (a) Gd_2S_3 phase and (b) A-RES phase in Y_2O_3 at 30 GPa.

not only significant persistent of C-RES during the transition process to B-RES but also the extensive pressure region where the B-RES phase was identified. As pointed out in the previous section, the transition was extremely sluggish at room temperature. Therefore, sufficient thermal energy would be substantial for refractory yttria to promote the transitions near the equilibrium phase boundaries. Such metastable behaviors in the high-pressure phase have also been observed in the C-RES phase in scandium sesquioxides.[16,28] The C-RES phase in Sc_2O_3 was reported to remain even over 30 GPa at room temperature, whereas a transition to the Gd_2S_3 phase was completed already at 18 GPa at high temperature.[16] The DFT computations revealed the Gd_2S_3 phase stabilized at high pressure with a transition pressure consistent to the well-annealed experiments.[16] Therefore, we should pay special attention to the kinetic effects on the phase transitions in the room-temperature experiments. Of course, they depend on the transition mechanism. Contrary to the reconstructive transition such as from B to Gd_2S_3, the B- to A-RES transition is expected to be displacive one as suggested for Eu_2O_3[29] and Sm_2O_3.[30,31]

Table 1. Lattice Parameters and Atomic Coordinates of B-RES ($C2/m$; $Z = 6$), A-RES ($P\bar{3}m1$; $Z = 1$), and Gd_2S_3 ($Pnma$; $Z = 4$) Phases Determined by DFT-LDA Computations

phase	site	x	y	z
B-RES	Y1	0.13517	0	0.48670
(0 GPa)	Y2	0.18991	0	0.13709
	Y3	0.46644	0	0.18735
	O1	0.02794	0	0.65612
	O2	0.29417	0	0.37549
	O3	0.32513	0	0.02923
	O4	0.37175	0	0.71647
	O5	0	0	0
lattice parameters	a = 13.6755 Å	b = 3.4501 Å	c = 8.4878 Å	β = 99.933°
B-RES	Y1	0.13562	0	0.48695
(10 GPa)	Y2	0.18748	0	0.13674
	Y3	0.46388	0	0.19044
	O1	0.02539	0	0.65469
	O2	0.29914	0	0.36838
	O3	0.32509	0	0.02672
	O4	0.36972	0	0.71143
	O5	0	0	0
lattice parameters	a = 13.2139 Å	b = 3.4224 Å	c = 8.3344 Å	β = 98.990°
B-RES	Y1	0.14188	0	0.52479
(20 GPa)	Y2	0.19144	0	0.14179
	Y3	0.47517	0	0.19154
	O1	0.00512	0	0.66160
	O2	0.33836	0	0.32833
	O3	0.32825	0	0.00507
	O4	0.33339	0	0.66672
	O5	0	0	0
lattice parameters	a = 12.3313 Å	b = 3.5439 Å	c = 8.1399 Å	β = 101.236°
A-RES	Y	0.33333	0.66667	0.23693
(30 GPa)	O1	0.33333	0.66667	0.65685
	O2	0	0	0
lattice parameters	a = 3.5383 Å		c = 5.1333 Å	
Gd_2S_3	Y1	0.15572	0.25	0.20137
(30 GPa)	Y2	0.76485	0.25	0.54774
	O1	0.51347	0.25	0.11154
	O2	0.63843	0.25	0.71999
	O3	0.86520	0.25	0.93634
lattice parameters	a = 5.6394 Å	b = 3.1743 Å	c = 12.0099 Å	

We depict the transition mechanism from B- to A-RES based on the atomic coordinates obtained by the DFT structural optimization (Table 1). The B-RES structure consists of three different yttrium sites (Figure 8a). Among them, only the Y3 site should be considered to possess a 6-fold oxygen coordination because the Y3−O2 distance (3.044 Å at 0 GPa) is too long to be classified into the 7-fold coordination (Figure 8a). Applying pressure, O2 moves closer toward Y3 and results in the formation of the 7-fold polyhedron. At 10 GPa, the Y3−O2 distance considerably shrinks from 3.044 to 2.819 Å, which is much more compressible than the other Y3−O distances. Upon further compression to 20 GPa, the Y3−O2 distance (2.195 Å) becomes shorter than the average Y3−O distance (2.261 Å); moreover, O1 moves into the *ac* plane

(29) Hyde, B. G.; Anderson, S. *Inorganic Crystal Structures*; Wiley: New York, 1989; pp245−247.

(30) Atou, T.; Kusaba, K.; Tsuchida, Y.; Utsumi, W.; Yagi, T.; Syono, Y. *Mater. Res. Bull.* **1989**, *24*, 1171.

(31) Atou, T.; Kusaba, K.; Syono, Y.; Kikegawa, T.; Iwasaki, H. In *High-Pressure Research Application to Earth and Planetary Sciences*; Terra Pub.: Tokyo, 1992; pp 469−475.

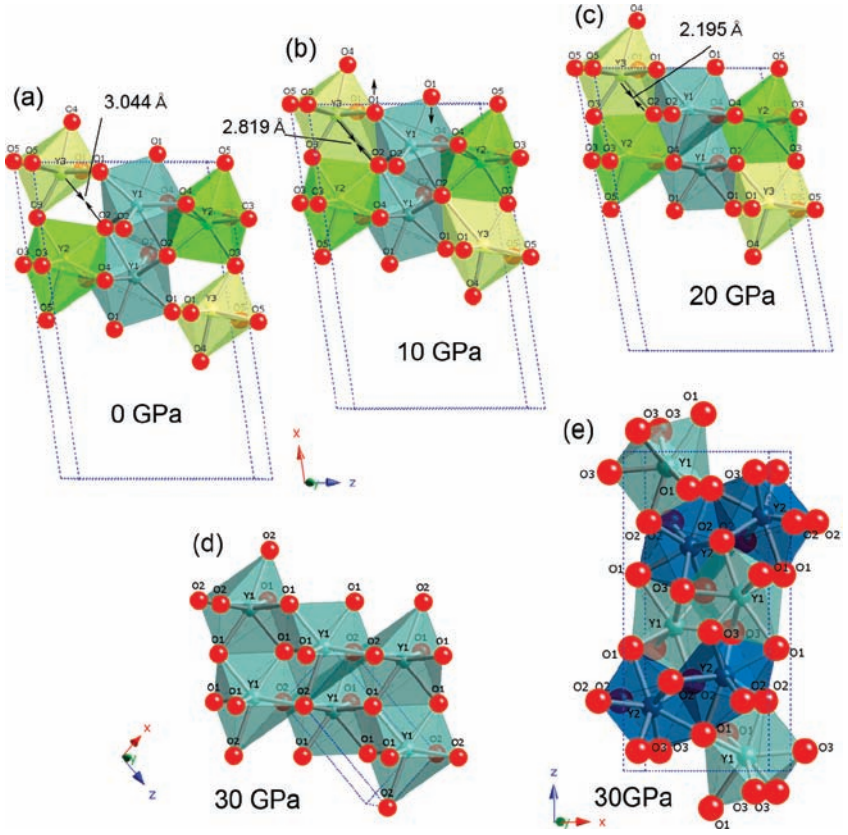

Figure 8. Clinographic views of crystal structures of (a) B-RES at atmospheric pressure, (b) B-RES at 10 GPa, (c) B-RES at 20 GPa, and (d) A-RES at 30 GPa. A part of a unit cell is shown for B-RES. The atomic coordinates and lattice parameters used are listed in Table 1. Small spheres at the center of polyhedra are yttrium, and large ones are oxygen. Each coordinated polyhedron is distinguished by different colors. The unit cell edges are indicated by dotted lines.

with almost the same x value as O5. Then, the B-RES structure finally changes to the one shown in Figure 8c at 20 GPa, which is found equivalent to the A-RES structure (Figure 8d). This means that A-RES can be derived directly from B-RES. In such a case, the transition is expected to proceed without kinetic delay even at room temperature. There is a group−subgroup relationship between $C2/m$ (B-RES) and $P\bar{3}m1$ (A-RES).[32] The transition from the B- to A-RES phases yields additional symmetry operations related to a triad axis. The metastable B- to A-RES transition pressure is estimated to be 9.5 GPa (LDA) and 20 GPa (GGA). This is quite consistent with some results of the room-temperature compression experiments. A recent ab initio computation study[28] indicated the B- to A-RES transition in Sc_2O_3 at 77 GPa. However, we already reported a discovery of the Gd_2S_3 phase above 18 GPa at high temperature.[16] Thus, similarity with the phase evolution in Y_2O_3 implies that the B- to A-RES transition in Sc_2O_3 would be achieved only metastably at low temperatures.

Equation of State Parameters and Structural Properties of Y_2O_3 Polymorphs. Figure 9 plots all the experimental $P-V$ data and the theoretical equation of states by LDA (Table 2) in order to compare the volumes of all Y_2O_3 polymorphs. We found a considerable density change (14%) from the C-RES to the Gd_2S_3 phase, which is thus obviously denser than A-RES. With respect to the cation−oxygen coordination, the coordination number (CN) of Y gradually increases from six in C-RES, to six and seven in B-RES, and finally to seven and eight in the Gd_2S_3 phase. On the other hand, the metastable A-RES

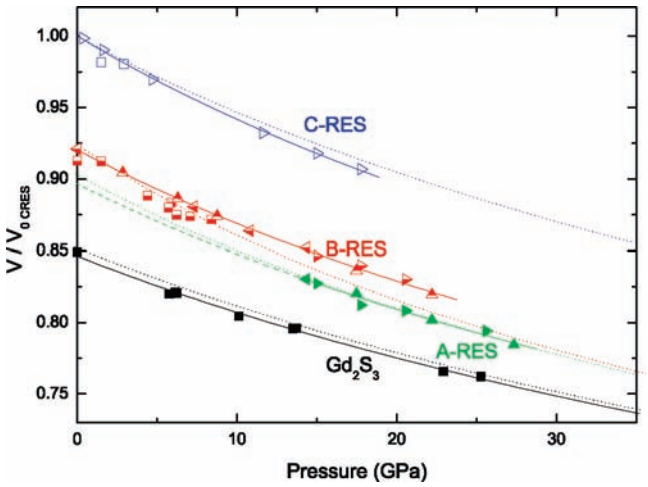

Figure 9. Compression curves and relative compression volume data ($V/V_{0\ \text{C-RES}}$) of Y_2O_3 polymorphs. Open (C-RES), half solid (B-RES), and solid (A-RES) triangles represent the room-temperature compression experimental data. Right, left, and up pointing triangles are obtained from the compression, decompression, and recompression experiments, respectively. Open (C-RES), half solid (B-RES), and solid (Gd_2S_3) squares represent the laser annealing experiments data. Solid lines are the results obtained by fitting the Birch−Murnaghan equation of state to the experimental data. Dotted lines are the results of DFT-LDA computations.

(32) Hahn, T. *International Table for Crystallography, A*, 5th ed.; Kluwer: Dordrecht, 2002; pp 540−541.

Table 2. Equation-of-State Parameters (B_0 and B_0') and Volumes (V_0) per Formula Unit

phase	V_0 (Å^3)	B_0 (GPa)[a]	B_0' [a]	method
C-RES	74.49(7)	147(2)	4[b]	XRD[c]
	71.58	163.5	3.98	DFT-LDA
B-RES	68.55(12)	155(4)	4[b]	XRD[c]
	66.16	117.9	4.83	DFT-LDA
A-RES	66.78(53)	159(15)	4[b]	XRD[c]
	64.63	144.6	4.37	DFT-LDA
Gd_2S_3	63.03(10)	191(5)	4[b]	XRD
	60.97	186.56	3.96	DFT-LDA
U_2S_3	61.25	178.89	4.30	DFT-LDA

[a] B_0 and B_0' are determined by fitting the Birch−Murnaghan equation of states to $P-V$ data. [b] Fixed value is used. [c] $P-V$ data obtained by quasihydrostatic compression experiments are used for the fitting.

Table 3. Effective Coordination Numbers (ECoN) and Distortion Indices (DI) of Oxygen-Coordinated Polyhedra and Their Connectivity with the Number of Neighboring Polyhedra

				no. of sharing types		
phase	polyhedra	ECoN	DI	corner	edge	face
B-RES (10 GPa)	YO_6	5.14	0.056	5	9	0
	YO_7	6.24	0.046	5	8	1
	YO_7	6.28	0.046	5	9	0
A-RES (30 GPa)	YO_7	6.11	0.055	3	12	0
Gd_2S_3 (30 GPa)	YO_7	6.72	0.027	5	10	1
	YO_8	7.79	0.021	9	4	5

structure possesses a seven oxygen coordination. Therefore, a volume reduction from A-RES to Gd_2S_3 (4%) is quite reasonable. Polyhedral types may also help to explain a large volume change from B-RES to Gd_2S_3. The effective coordination numbers (ECoN)[33,34] and the distortion index (DI)[34,35] of polyhedra are useful indicators to understand how polyhedra deviate from their ideal forms (Table 3). The ECoN clearly indicates that the coordination numbers of polyhedra in B-RES are close to five and six rather six and seven. According to DI, a significant polyhedral distortion causes the deviation from the classical CN. In contrast, the ECoNs of polyhedra in the Gd_2S_3 phase are very close to their classical CN values. This is the reason why the transition from B-RES to Gd_2S_3 yields quite a large volume change. We should also consider the polyhedra connectivity. The polyhedra in the Gd_2S_3 structure share their six faces. In contrast, the polyhedra in the B-RES structure share only a face. Increase in the face sharing connectivity also plays an important role on the densification. Interestingly, the ECoN in the A-RES phase is much lower than seven (Table 3) as well as B-RES. This is reasonable because of the simple structural relationship between A-RES and B-RES.

Metastable Structures Recovered from the Gd_2S_3 Phase of III Sesquioxides. So far, we have found three sesquioxides, In_2O_3, Sc_2O_3, and Y_2O_3, crystallizing into the Gd_2S_3 structure under high pressure. Here, we focus on their structural changes during decompression. Our previous studies[15,16] suggest that the Gd_2S_3 structure in In_2O_3[15] and Sc_2O_3[16] metastably converted into the corundum structure rather than the stable C-RES structure during decompression at room temperature. Our theoretical considerations indicated that the corundum phases are metastable products.[15,16] In the present Y_2O_3, some samples retained the Gd_2S_3 structure even after releasing pressure without corundum formation. The C-RES phase is thermodynamically stable at ambient pressure in all three compounds. As indicated in Figure 10, enthalpy differences between C-RES and corundum are not large (ΔH = 11.6, 19.6, and 23.4 kJ/mol for In_2O_3, Sc_2O_3, and Y_2O_3, respectively); meanwhile, there are significant enthalpy differences between the C-RES and the Gd_2S_3 phases (ΔH = 97.0, 52.8, and 30.4 kJ/mol for In_2O_3, Sc_2O_3, and Y_2O_3, respectively). The large enthalpy difference between C-RES and Gd_2S_3 implies the Gd_2S_3 structure is less easily maintained in In_2O_3 and Sc_2O_3; therefore, the Gd_2S_3 may transform into the intermediate corundum structure under decompression. In contrast, the enthalpy difference in Y_2O_3 is much smaller, which would be enough to retain the Gd_2S_3 structure even at ambient pressure.

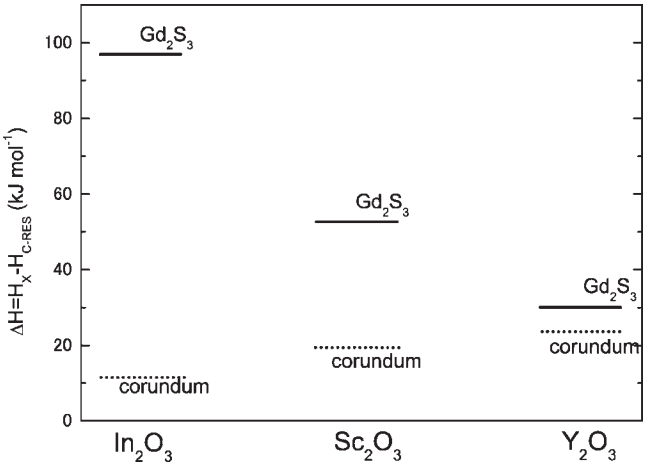

Figure 10. Enthalpy differences relative to C-RES for corundum (dotted lines) and Gd_2S_3 phases (solid lines) in In_2O_3,[15] Sc_2O_3,[16] and Y_2O_3 (present study) at ambient pressure.

In these sesquoxides, the zero-pressure enthalpy difference between Gd_2S_3 and corundum phase seems to correlate with the degree of covalence which is clearly demonstrated in the electronegativities.[36] The enthalpy difference would decrease as the electronegativities of cations decrease. If this postulate crystal chemically makes sense, it would be useful to guess a compound which has a perfectly quenchable Gd_2S_3 phase.

Summary

High-pressure experiments and ab initio calculations revealed that (1) the Gd_2S_3 structure is the densest phase in Y_2O_3 polymorphs, (2) the displacive phase transition from B- to A-RES occurs metastably at room temperature, (3) the high temperature implemented by a laser heated DAC eclipses the appearance of A-RES phase under high pressure, (4) Gd_2S_3 type yttria can be partially quenched at ambient pressure, and (5) the band gap is reduced by the B-RES to Gd_2S_3 transition in Y_2O_3.

(33) Hoppe, R. *Z. Kristallogr.* **1979**, *150*, 23.
(34) Momma, K.; Izumi, F. *Comission on Crystallogr. Comput., IUCr Newslett.* **2006**, No. 7:106; a program VESTA performs calculations of ECoN.
(35) Baur, W. H. *Acta Crystallogr. B* **1974**, *30*, 1195.
(36) Pauling, L. *The Nature of the Chemical Bond*; Cornell University Press: Ithaca, 1960; pp 93.

Acknowledgment. H.Y. acknowledges supports from NIMS Competitive Research Funds and NIMS Exploratory Research Funds. We acknowledge supports from Grant-in-Aid for Scientific Research from JSPS (No. 22340164 to H.Y. and Nos. 21740379 and 20001005 to T.T.), and GCOE program at Ehime University. The synchrotron radiation experiments were conducted at BL-10XU in SPring-8 with the approval of JASRI (Proposal Nos. 2008A1253 and 2009A1216), and the ab initio calculations were performed using the GRC-Parallel Computing System. We also thank Sara Whitaker for helpful corrections of the manuscript.